Reconstruction of Current Distribution on a Given Conductor Structure Using Frequency Domain Near-Field Data without Phase Information

Robert Nowak, Stephan Frei
TU Dortmund University
Dortmund, Germany
robert.nowak@tu-dortmund.de

***Abstract*—Information on field emissions is required in many applications. Typically, antennas are used for the measurement of the far-field. Antenna measurements suffer from several problems, e.g. the need of large anechoic chambers. Near-field measurements/scans might become an attractive alternative in the future. The far-field can finally be calculated from near-field measurement data. For an accurate calculation, phase and amplitude distributions of the near-fields are needed for all considered frequencies. As phase measurement can be very troublesome, the reconstruction of the phase from phase-less measurement data is highly attractive. In this paper, a method is presented to find the EMI of PCB traces or similar structures with phase-less near-field measurements. In this method, knowledge of the geometry of potential radiating is applied. From this knowledge, boundary conditions can be found for phase estimation. The method is shown in detail and the benefits are discussed on result of reconstructed current distributions and estimations of the far-field.**

Keywords—source reconstruction; iterative reconstruction; current distribution; near-field; EMI analysis; far-field

I. INTRODUCTION

The usage of near-field scan data is highly attractive for EMI-analysis due to several reasons [1] – [3]. Large anechoic chambers are not needed for such analysis. The far-field can be computed or detailed information on the radiation sources can be obtained. Radiation sources like printed circuit boards (PCBs) can be analyzed. From the near-field data, radiating structures (mostly conducting traces) can be identified and suitable design changes can be found. This method is especially advantageous during hardware development, since potential EMC issues can be identified and resolved early.

In this work, a field source model of a radiating known geometrical structure is developed from near-field scan data and is used to identify the radiating structure's electrical parameters. The intention of this approach is the estimation of the radiated emissions from a PCB and isolating the root cause.

Different field source models can be used. One approach is the usage of a set of dipoles, arranged in a regular grid, to represent the radiation of PCBs, e.g. [3] – [6]. Depending on the scan data quality, and the complexity of the investigated structure, promising results could be achieved [3]. However, finding the root cause of an EMI problem is difficult, as the dipole sources cannot be assigned easily directly to a radiating PCB trace.

Another approach to design a field source model is based on geometry information. As presented in [1], [7], [8], the dipoles are arranged according to the possible current paths of an investigated structure (e.g. PCB). In contrast to the approach using a regular grid arrangement, the parameterized models may include additional information like the current distribution. Therefore, methods using this model approach are often referred to as *current reconstruction methods*.

If accurate near-field data with phase information is available, the parametrization of the field source model can be performed directly by solving an inverse problem [6] – [8]. As shown, e.g. in [6] or [9], the measurement of the phase is troublesome. Therefore, reconstructing the phase from phase-less measurement data is an attractive alternative. To do so, iterative algorithms can be used [4], [5]. Another approach is proposed in [10]. Using near-field data on two parallel planes, an iteration-free phase estimation can be found. In contrast to iterative algorithms, this approach has very high demands on the accuracy of a measurement in the distant plane.

In this paper, a further elaborated current reconstruction method is presented. Only the information on the possible current paths has been used in previous approaches. In this work, additional information on the system is considered. This information includes on the one hand the behavior of termination circuits. On the other hand, an approach to define possible ranges of the investigated system's quantities is presented. An iterative process is presented to parameterize the extended model based on phase-less near field data. No special requirements on the arrangement of the measurement points need to be considered. In this work, the near-field data is given in an equally spaced grid on a single plane. Analyzing an exemplary structure, the benefit of considering additional information on the system is discussed. Here, results for reconstructed current distribution and estimations of the far-field are investigated.

In II and III, the basic model approach and the iterative process to evaluate phase-less near-field data are presented. Next In IV, the integration of additional conditions is shown. The derived method is applied on simulation data in V. A conclusion and an outlook close the work.

II. INVERSE PROBLEM FOR THE RECONSTRUCTION OF THE CURRENT DISTRIBUTION

One essential part of the inverse problem is the description of the relation between the current distribution and the near-field. A set of electric dipoles can be used as flexible model to map a measured field. As shown already in [8] a conductor-system on a PCB can be subdivided in N short segments, to each segment a dipole with current I_n can be assigned (see Fig. 1). The magnetic field of every dipole can be calculated easily. Hence, the current I_n of the n^{th} segment generates a magnetic field $\mathbf{H}_\mathrm{m}$ at the m^{th} observation point. This can be formulated in Cartesian components:

$$\begin{bmatrix} H_{\mathrm{x,m}} \\ H_{y,\mathrm{m}} \\ H_{\mathrm{z,m}} \end{bmatrix} = \begin{bmatrix} \psi_{\mathrm{x,nm}} \\ \psi_{\mathrm{y,nm}} \\ \psi_{\mathrm{z,nm}} \end{bmatrix} \cdot I_{\mathrm{n}} \Leftrightarrow \mathbf{H}_{\mathrm{m}} = \boldsymbol{\psi}_{\mathrm{nm}} \cdot I_{\mathrm{n}} \tag{1}$$

The components of $\boldsymbol{\psi}_{\mathrm{nm}}$ are the magnetic field function for an electric dipole. The lengths of the n^{th} segment in the different spatial directions are included as dipole lengths [8], [11]. According to this description, the superposition of the magnetic fields for all M observation points of all N segment currents is

$$\begin{bmatrix} \mathbf{H}_1 \\ \vdots \\ \mathbf{H}_{\mathrm{M}} \end{bmatrix} = \begin{bmatrix} \boldsymbol{\psi}_{11} & \cdots & \boldsymbol{\psi}_{1\mathrm{N}} \\ \vdots & \ddots & \vdots \\ \boldsymbol{\psi}_{\mathrm{M1}} & \cdots & \boldsymbol{\psi}_{\mathrm{MN}} \end{bmatrix} \cdot \begin{bmatrix} I_1 \\ \vdots \\ I_{\mathrm{N}} \end{bmatrix} \Leftrightarrow \mathbf{H} = \boldsymbol{\Psi}_{\mathrm{IH}} \cdot \mathbf{I}\,. \tag{2}$$

This formula gives the relation between the magnetic near-field and the generating current distribution. Formulas to calculate the far-field of a known current distribution can be formulated similarly.

In (2), an inverse formulation for the current distribution is given if sufficient magnetic field data points are given. To reduce the complexity, segment currents on short sections of the conductors can assumed to be constant. For longer sections transmission line theory can be used, with incident and reflected current waves. The currents $I_{\mathrm{p,k}}, I_{\mathrm{p+1,k}}, \cdots, I_{\mathrm{q,k}}$ of the k^{th} section can be fixed. If a section is short, e.g. section k_1 in Fig. 1, the assignment

$$\begin{bmatrix} I_{\mathrm{p,k}} \\ \vdots \\ I_{\mathrm{q,k}} \end{bmatrix} = \begin{bmatrix} 1 \\ \vdots \\ 1 \end{bmatrix} \cdot I_{\mathrm{c,k}} \tag{3}$$

with the constant current $I_{\mathrm{c,k}}$ can be used. For longer sections, like section k_2 in Fig. 1, using the propagation constant γ_{k} of the k^{th}section, the current distribution can be represented with

$$\begin{bmatrix} I_{\mathrm{p,k}} \\ \vdots \\ I_{\mathrm{q,k}} \end{bmatrix} = \begin{bmatrix} \mathrm{e}^{-\gamma_{\mathrm{k}} d_{\mathrm{p,k}}} & -\mathrm{e}^{\gamma_{\mathrm{k}} d_{\mathrm{p,k}}} \\ \vdots & \vdots \\ \mathrm{e}^{-\gamma_{\mathrm{k}} d_{\mathrm{q,k}}} & -\mathrm{e}^{\gamma_{\mathrm{k}} d_{\mathrm{q,k}}} \end{bmatrix} \cdot \begin{bmatrix} I_{\mathrm{i,k}} \\ I_{\mathrm{r,k}} \end{bmatrix}. \tag{4}$$

In this equation, the position $d_{\mathrm{n,k}}$ of the n^{th} segment is chosen on the center of the segment on a coordinate system oriented in section direction. Here, the positions $d_{\mathrm{S,k}}$ and $d_{\mathrm{E,k}}$ denote the start and end positions of the k^{th} section. Finally, merging the conditions given in (3) and (4) in the matrix $\boldsymbol{\Psi}_{\mathrm{TL}}$, the inverse problem of (2) is represented in

$$\mathbf{H} = \boldsymbol{\Psi}_{\mathrm{IH}} \cdot \boldsymbol{\Psi}_{\mathrm{TL}} \cdot \mathbf{I}_{\mathrm{S}} \tag{5}$$

with the current vector

$$\mathbf{I}_{\mathrm{S}} = [I_{\mathrm{i,1}} \quad I_{\mathrm{r,1}} \quad \cdots \quad I_{\mathrm{i,P}} \quad I_{\mathrm{r,P}} \quad I_{\mathrm{c,1}} \quad \cdots \quad I_{\mathrm{c,Q}}]^{\mathrm{T}}\,. \tag{6}$$

III. Evaluating Phase-Less Near-Field Data by Iterative Solution of the Inverse Problem

In the inverse problem of (2) respectively (5) both, magnetic field and the generating current values, are complex values. If the magnetic field is known by magnitude and phase, the least squares solution $\hat{\mathbf{I}}_{\mathrm{S}}$ of

$$\hat{\mathbf{I}}_{\mathrm{S}} = \arg\min_{\mathbf{I}_{\mathrm{S}}} \|\boldsymbol{\Psi}_{\mathrm{IH}} \cdot \boldsymbol{\Psi}_{\mathrm{TL}} \cdot \mathbf{I}_{\mathrm{S}} - \mathbf{H}\|_2 \tag{7}$$

describes the requested current distribution. However, if only magnitude of field distribution is given, the single evaluation of (7) does not generally lead to a correct solution. To solve this problem, an iterative algorithm is used, that corresponds

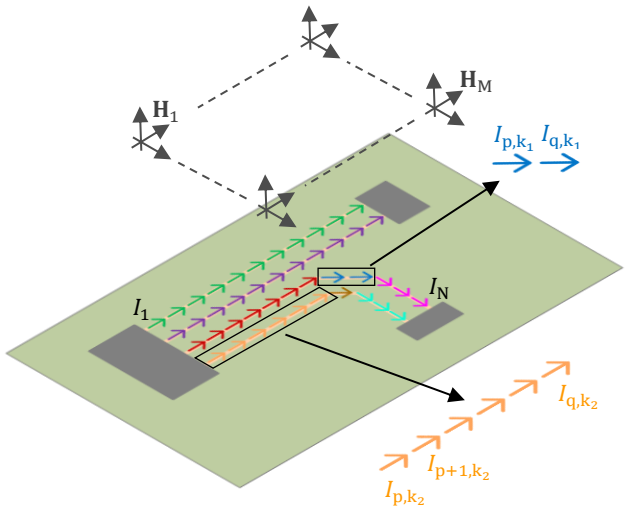

Fig. 1. Example field source model of the conductor system on a PCB.

with the basic idea of the methods presented in [4] and [5]. The algorithm is described in the following.

First, an arbitrary phase $\boldsymbol{\varphi}^{(0)}$ is assumed for the measured magnetic field $\mathbf{H}^{\mathrm{Magn}}$ that is only given by its magnitude. Thus, the magnetic field at M field points is described by

$$\mathbf{H}^{\mathrm{Magn}} \in \mathbb{R}^{3\mathrm{M}\times 1} \tag{8}$$

and the phases are for the moment presented as

$$\boldsymbol{\varphi}^{(0)} = \left[\left[\varphi_{\mathrm{x,m}}^{(0)} \quad \varphi_{\mathrm{y,m}}^{(0)} \quad \varphi_{\mathrm{z,m}}^{(0)}\right]^{\mathrm{T}}\right]_{\mathrm{k}\,\in\,\mathrm{M}\times 1}. \tag{9}$$

The resulting initial near-field is

$$\begin{aligned} &\mathbf{H}^{(0)} = \mathbf{H}^{\mathrm{Magn}} \circ \mathrm{e}^{\mathrm{j}\boldsymbol{\varphi}^{(0)}} \\ &\Leftrightarrow \begin{bmatrix} H_{\mathrm{x,m}}^{(0)} \\ H_{\mathrm{y,m}}^{(0)} \\ H_{\mathrm{z,m}}^{(0)} \end{bmatrix} = \begin{bmatrix} H_{\mathrm{x,m}}^{\mathrm{Magn}} \cdot \mathrm{e}^{\mathrm{j}\varphi_{\mathrm{x,m}}^{(0)}} \\ H_{\mathrm{y,m}}^{\mathrm{Magn}} \cdot \mathrm{e}^{\mathrm{j}\varphi_{\mathrm{y,m}}^{(0)}} \\ H_{\mathrm{z,m}}^{\mathrm{Magn}} \cdot \mathrm{e}^{\mathrm{j}\varphi_{\mathrm{z,m}}^{(0)}} \end{bmatrix} \quad \forall\, m \in \mathbb{N}_{\mathrm{M}}^{*}\,. \end{aligned} \tag{10}$$

Using this data, a current distribution can be determined by the least squares' solution of

$$\hat{\mathbf{I}}_{\mathrm{S}}^{(\mathrm{i})} = \arg\min_{\mathbf{I}_{\mathrm{S}}} \left\|\boldsymbol{\Psi}_{\mathrm{IH}} \cdot \boldsymbol{\Psi}_{\mathrm{TL}} \cdot \mathbf{I}_{\mathrm{S}} - \mathbf{H}^{(\mathrm{i}-1)}\right\|_2 \quad \forall\, i \in \mathbb{N}^{*}\,. \tag{11}$$

According to (5), the estimated new values $\hat{\mathbf{I}}_{\mathrm{S}}^{(\mathrm{i})}$ of the i^{th} iteration step give the new magnetic field approximation

$$\hat{\mathbf{H}}^{(\mathrm{i})} = \boldsymbol{\Psi}_{\mathrm{IH}} \cdot \boldsymbol{\Psi}_{\mathrm{TL}} \cdot \hat{\mathbf{I}}_{\mathrm{S}}^{(\mathrm{i})}\,. \tag{12}$$

The phase information

$$\boldsymbol{\varphi}^{(\mathrm{i})} = \arg \hat{\mathbf{H}}^{(\mathrm{i})} \tag{13}$$

of this model is combined with the basic information about the magnitude of the magnetic field:

$$\mathbf{H}^{(\mathrm{i})} = \mathbf{H}^{\mathrm{Magn}} \circ \mathrm{e}^{\mathrm{j}\boldsymbol{\varphi}^{(\mathrm{i})}} \tag{14}$$

Using this resulting field data, a new current vector $\hat{\mathbf{I}}_{\mathrm{S}}^{(\mathrm{i}+1)}$ can found solving (11).

For starting the iteration process, an initial guess for the phase distribution $\boldsymbol{\varphi}^{(0)}$ (9) must be given. Assuming convergence of the presented algorithm, the number of iteration steps required to obtain a solution depends on the

initial guess of the phase distribution. In addition, the iterative algorithm is able to converge to different solutions and the found solutions depend on the initial value. Investigations with different sets of initial values have shown that random numbers give good results. Here, further research is needed. For $\boldsymbol{\varphi}^{(0)}$ an initial random phase distribution $[0, 2\pi]$ is used:

$$\varphi_{\{\mathrm{x,y,z}\},\mathrm{k}}^{(0)} \sim \mathcal{U}(0{,}2\pi)\ \forall\ k \in \mathbb{N}_{\mathrm{M}}^{*} \tag{15}$$

To terminate the iteration process, two criterions can be applied. The first criterion is based on the solution of the inverse problem. Here, the mean value of the relative deviation of the solution $\hat{\mathbf{I}}_{\mathrm{S}}$ from two successive iteration steps is used:

$$\sigma_{\mathrm{rel,sol}}^{(\mathrm{i})} = \frac{1}{K} \cdot \sum_{k=1}^{K} \left| \frac{\hat{I}_{\mathrm{k}}^{(i)} - \hat{I}_{\mathrm{k}}^{(i-1)}}{\hat{I}_{\mathrm{k}}^{(i)}} \right|, \hat{\mathbf{I}}_{\mathrm{S}}^{(\mathrm{i})} = \left[\hat{I}_{\mathrm{k}}^{(i)}\right]_{\mathrm{k}\,\in\,\mathrm{K}\times 1} \tag{16}$$

The second criterion is based on the deviation of the phase of the reconstructed magnetic field. Considering the periodicity of the phase information, the criterion can be formulated as

$$\sigma_{\mathrm{phs}}^{(\mathrm{i})} = \frac{1}{3M} \sum_{m=1}^{M} \sum_{\mathrm{dir}=\{\mathrm{x,y,z}\}} \left| \mathrm{e}^{j \arg\left(\hat{H}_{\mathrm{dir,m}}^{(\mathrm{i})}\right)} - \mathrm{e}^{j \arg\left(\hat{H}_{\mathrm{dir,m}}^{(\mathrm{i}-1)}\right)} \right|. \tag{17}$$

The relative variation of the solution is described by both criterions. Therefore, they can be applied to formulate an effective termination condition.

IV. Implementation of Network Equations in the Inverse Problem

The solution of the least-square problem in (7) or (11) leads generally to a solution, the residuum of (5) is minimized, but it might not reflect the physical reality of the measured system. In this section, the formulation of additional boundary conditions is introduced to improve the solution's quality.

A. Formulation of Network Equations in the Inverse Problem

First, the investigated conductor system forms an electric network, Kirchhoff's circuit laws must be valid. To formulate these laws as additional conditions for the problem, the incident and reflected waves of the transmission-line equations in (6) must be represented as currents and voltages at the ends of the conductors. Thus, the voltages and currents at the start and end of the k^{th} conductor are given by

$$\begin{bmatrix} V_{\mathrm{S,k}} \\ I_{\mathrm{S,k}} \\ V_{\mathrm{E,k}} \\ I_{\mathrm{E,k}} \end{bmatrix} = \underbrace{\begin{bmatrix} Z_{0,\mathrm{k}}\mathrm{e}^{-\gamma_{\mathrm{k}} d_{\mathrm{S,k}}} & Z_{0,\mathrm{k}}\mathrm{e}^{\gamma_{\mathrm{k}} d_{\mathrm{S,k}}} \\ \mathrm{e}^{-\gamma_{\mathrm{k}} d_{\mathrm{S,k}}} & -\mathrm{e}^{\gamma_{\mathrm{k}} d_{\mathrm{S,k}}} \\ Z_{0,\mathrm{k}}\mathrm{e}^{-\gamma_{\mathrm{k}} d_{\mathrm{E,k}}} & Z_{0,\mathrm{k}}\mathrm{e}^{\gamma_{\mathrm{k}} d_{\mathrm{E,k}}} \\ \mathrm{e}^{-\gamma_{\mathrm{k}} d_{\mathrm{E,k}}} & -\mathrm{e}^{\gamma_{\mathrm{k}} d_{\mathrm{E,k}}} \end{bmatrix}}_{=\mathbf{K}_{\mathrm{k}}} \cdot \begin{bmatrix} I_{\mathrm{i,k}} \\ I_{\mathrm{r,k}} \end{bmatrix}. \tag{18}$$

Here, $Z_{0,\mathrm{k}}$ is the wave impedance of each conductor. Using the transformation matrices $\mathbf{K}_{\mathrm{k}}$ for all conductors lead to the following network values:

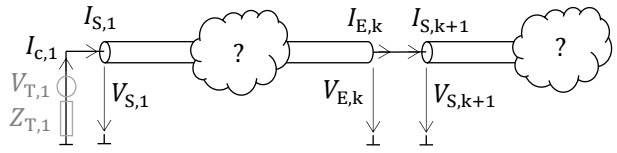

Fig. 2. Example conductor system

$$\begin{bmatrix} \begin{bmatrix} V_{\mathrm{S,1}} \\ I_{\mathrm{S,1}} \\ V_{\mathrm{E,1}} \\ I_{\mathrm{E,1}} \end{bmatrix}^{\mathrm{T}} \cdots \begin{bmatrix} V_{\mathrm{S,P}} \\ I_{\mathrm{S,P}} \\ V_{\mathrm{E,P}} \\ I_{\mathrm{E,P}} \end{bmatrix}^{\mathrm{T}} \begin{bmatrix} I_{\mathrm{c,1}} \\ \vdots \\ I_{\mathrm{c,Q}} \end{bmatrix}^{\mathrm{T}} \end{bmatrix}^{\mathrm{T}} = \underbrace{\begin{bmatrix} \mathbf{K}_1 & & \\ & \ddots & \\ & & \mathbf{K}_{\mathrm{P}} \\ & & \mathbf{E} \end{bmatrix}}_{=\mathbf{K}_{\mathbf{T}}} \begin{bmatrix} I_{\mathrm{i,1}} \\ I_{\mathrm{r,1}} \\ \vdots \\ I_{\mathrm{i,P}} \\ I_{\mathrm{r,P}} \\ I_{\mathrm{c,1}} \\ \vdots \\ I_{\mathrm{c,Q}} \end{bmatrix} \tag{19}$$

Now, it is possible to formulate Kirchhoff's circuit law. The approach is now explained further based on the configuration showed in Fig. 2, the corresponding relations are represented in the following equation:

$$\begin{bmatrix} & 1 & & & & & & & -1 & \\ & & \cdots & 1 & 0 & -1 & 0 & \cdots & & \cdots \\ & & & 0 & 1 & 0 & -1 & & & \\ 1 & \mathrm{Z}_{\mathrm{T,1}} & & & & & & & & \end{bmatrix} \cdot \\ [V_{\mathrm{S,1}}\ \ I_{\mathrm{S,1}}\ \cdots\ V_{\mathrm{E,k}}\ \ I_{\mathrm{E,k}}\ \ V_{\mathrm{S,k+1}}\ \ I_{\mathrm{S,k+1}}\ \cdots\ I_{\mathrm{c,1}}\ \cdots]^{\mathrm{T}} \\ = [0\ \ 0\ \ 0\ \ V_{\mathrm{T,1}}]^{\mathrm{T}} \tag{20}$$

The first row of the matrix in (20) represents the nodal rule at the presented vertical element and the first line. Similar to this, the nodal rule between line k and $k+1$ is expressed in row 3. In addition, the continuity of the voltage at the end and start of the lines is formulated as equation in the second row. Row 4 represents a termination conditions by considering a Thévenin equivalent circuit. If the equivalent impedance and voltage source of the network is known, this information can be used as additional condition.

B. Implementation of Conditions in the Inverse Problem Formulation

There are many methods to solve a least-squares problem considering additional conditions. As the investigated problem here is based on complex numbers the inverse problem and the additional conditions have to be separated in real and imaginary part:

$$\begin{aligned} &\boldsymbol{\Psi} \cdot \mathbf{I}_{\mathrm{S}} = \mathbf{H}, \qquad \boldsymbol{\Psi} = \boldsymbol{\Psi}_{\mathrm{HI}} \cdot \boldsymbol{\Psi}_{\mathrm{TL}} \\ &\Leftrightarrow (\boldsymbol{\Psi}_{\mathrm{Re}} + \mathrm{j}\boldsymbol{\Psi}_{\mathrm{Im}}) \cdot \left(\mathbf{I}_{\mathrm{S,Re}} + \mathrm{j}\mathbf{I}_{\mathrm{S,Im}}\right) = (\mathbf{H}_{\mathrm{Re}} + \mathrm{j}\mathbf{H}_{\mathrm{Im}}) \end{aligned} \tag{21}$$

Comparing real and imaginary parts of this equation, the problem can also be formulated with

$$\begin{bmatrix} \boldsymbol{\Psi}_{\mathrm{Re}} & -\boldsymbol{\Psi}_{\mathrm{Im}} \\ \boldsymbol{\Psi}_{\mathrm{Im}} & \boldsymbol{\Psi}_{\mathrm{Re}} \end{bmatrix} \cdot \begin{bmatrix} \mathbf{I}_{\mathrm{S,Re}} \\ \mathbf{I}_{\mathrm{S,Im}} \end{bmatrix} = \begin{bmatrix} \mathbf{H}_{\mathrm{Re}} \\ \mathbf{H}_{\mathrm{Im}} \end{bmatrix}. \tag{22}$$

To solve the resulting real least-square problem, an interior-point-convex algorithm is used [12]. Here, the additional conditions shown in (20) must also be formulated considering real and imaginary part.

C. Consideration of Limits in the Inverse Problem

The solution of the problem in the form of (22) with classical methods also allows the consideration of inequality conditions like

$$\begin{aligned} &\mathbf{A}_{\mathrm{Lim}} \cdot \mathbf{x} \leq \mathbf{b}_{\mathrm{Lim}}, \\ &\qquad \mathbf{A}_{\mathrm{Lim}} \in \mathbb{R}^{\mathrm{F}\times\mathrm{G}}, \mathbf{x} \in \mathbb{R}^{\mathrm{F}\times 1}, \mathbf{b}_{\mathrm{Lim}} \in \mathbb{R}^{\mathrm{G}\times 1}, \\ &\Leftrightarrow A_{\mathrm{Lim,i,1}}\, x_{\mathrm{i}} + \cdots + A_{\mathrm{Lim,i,F}}\, x_{\mathrm{F}} \leq b_{\mathrm{i}} \quad \forall\ 1 \leq i \leq G \end{aligned} \tag{23}$$

This option can be used to set limitations on unknown values. To introduce reasonable limits, the usage of the transformation matrix $\mathbf{K}_{\mathrm{T}}$ represented in real and imaginary part like in (22) can be helpful. This way limit conditions (23)

for currents and voltages in the investigated conductor system can be given.

The most useful limitation on a value is the limitation of the norm respectively the magnitude, e.g. in the case of the voltage $V_{T,i}$ at the end of a line:

$$\left|V_{T,i}\right| \lesssim V_{Max} \tag{24}$$

Formulating linear conditions on the real and imaginary part of $V_{T,i}$, following equations can be used to fulfill this requirement:

$$\begin{bmatrix} \vdots & & & & & & & \\ 1 & -1 & -1 & 1 & 1 & -1 & 0 & 0 \\ \vdots & & & & & & & \\ 1 & -1 & 1 & -1 & 0 & 0 & 1 & -1 \\ \vdots & & & & & & & \end{bmatrix}^{T} \cdot \begin{bmatrix} \vdots \\ \mathrm{Re}\{V_{T,i}\} \\ \vdots \\ \mathrm{Im}\{V_{T,i}\} \\ \vdots \end{bmatrix} \lesssim V_{Max} \cdot [\sqrt{2} \quad \sqrt{2} \quad \sqrt{2} \quad \sqrt{2} \quad 1 \quad 1 \quad 1 \quad 1]^{T} \tag{25}$$

In Fig. 3, the set of possible values of $V_{T,i}$ are shown. Having the form of an octagon, the set approximately fits to the demanded form of a circle.

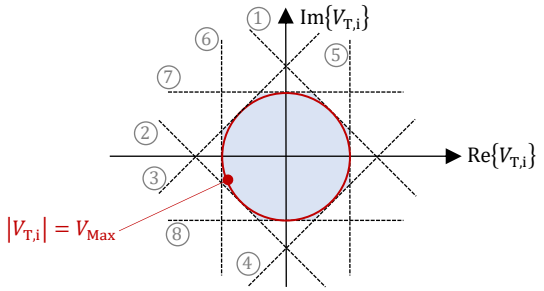

Fig. 3. Illustration of the possible values of $V_{T,i}$ described by (25) with the representation of the limiting rows of the inequation system.

V. Application on Simulation Data

In this chapter, a simulation setup is investigated with the presented methods. Afterward, the achieved results are discussed.

A. Setup

In Fig. 4, the investigated conductor system is shown. The near-ends of the six lines are marked with numeric labels. All conductors are stimulated by a Thévenin circuit at the near-end. The stimulus and the terminations at the far-ends are listed in table I. Arranged above an ideal infinite ground plane, all lines have a height of 1.5 mm. The terminations are assumed along the vertical conductors that connect the conductors to a ground plane. All conductors have a radius of 0.1 mm.

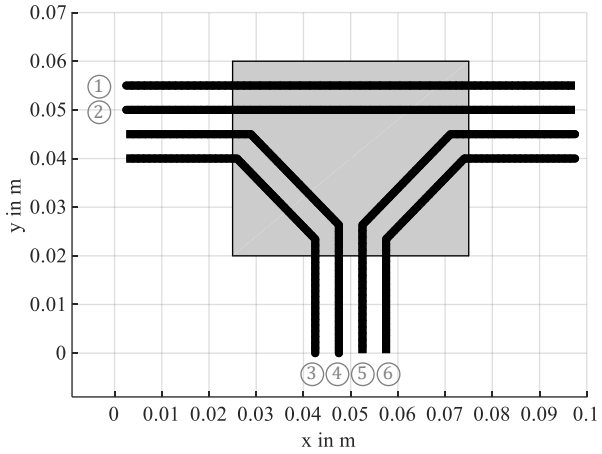

Fig. 4. Investigated conductor system (black) and area of used near-field data (grey)

For modeling and simulation CONCEPT-II [13] is used. The magnetic near-field is computed on an equally spaced grid 7 mm above the ground plane in the grey area shown in Fig. 4. Having a spacing of 5 mm, the grid contains 99 field points that are used for the application of the reconstruction methods. In order to investigate the influence of measurement noise the simulated data is modified by adding a noise signal with a magnitude of 70 $\mathrm{dB}_{\mu\mathrm{Am}^{-1}}$ varying the amplitude about ± 2 dB.

Three variants of the presented current reconstruction method are used. The first variant only uses the network equations to obtain a continuous current distribution. In the second variant, the magnitude limitation is additionally used. Here, the voltage of every near- and far-end of the conductors is limited by the exciting voltage source, e.g. for line 3 the condition $|V_S| \lesssim 5$ V is given. The third variant also uses the network equations and information about the termination circuits. Here, only the impedance information of the far-end terminations without any estimation of additional parasitic effects are taken into account. In table II, an overview of the described variants is presented.

TABLE I.
Circuits At Near-End and Far-End of Exemplary Conductor System

conductor number	stimulus (near end)	termination (far end)	number of dipoles
1	1 V $e^{j90°}$, 10 Ω	100 Ω	66
2	1 V $e^{j90°}$, 10 Ω	100 Ω	66
3	5 V $e^{j0°}$, 50 Ω	50 Ω	66
4	5 V $e^{j180°}$, 50 Ω	50 Ω	66
5	3 V $e^{j0°}$, 50 Ω	50 Ω	66
6	3 V $e^{j0°}$, 50 Ω	50 Ω	66

TABLE II.
Considered Conditions in the Applied Variants of the Current Reconstruction Method

	Variant 1	Variant 2	Variant 3
Kirchhoff's circuit laws[a.]	✓	✓	✓
Limitation of values		✓	
Using termination information			✓
Color in plots	blue	yellow	green

[a.] Kirchhoff's circuits law is considered in all presented investigations

B. Application on Near-Field Data with Phase Information

In the first investigation, the presented method is validated in principle. All three variants are applied on simulation data containing noise and phase information. In Fig. 5, the reconstructed current distribution for 100 MHz is exemplary shown for conductor 1, 3 and 5. Overall, all approaches lead to a useful result about the magnitude of the floating current although the raw data contain noise. In particular, the second and third variant calculate a distribution that is very similar to the simulated currents.

C. Application on Phaseless Near-Field Data

After a general proof of concept, in this chapter the reconstructed current distributions for several frequencies are shown. For all investigation in this section, near-field data without phase information is used. Thus, the iterative process of III is applied. The condition

$$\sigma^{(\mathrm{i})}_{\mathrm{abs,Magn}} < 1\,‰ \;\&\; \sigma^{(\mathrm{i})}_{\mathrm{phs}} < 1\,‰ \tag{26}$$

is used as stop criterion, and only 300 iteration steps are allowed. In the investigation, the phase of the current distribution is compared as well. For this comparison, the phase of the current at the far-end termination of conductor 5 is assumed as zero for both, reconstructed and simulated current distribution.

First, general evaluations of the iterative process are presented. Here, a conductor system is investigated for an excitation of 1 GHz. The iterative algorithm is applied 100 times with different initial phase distributions. In Fig. 6, the

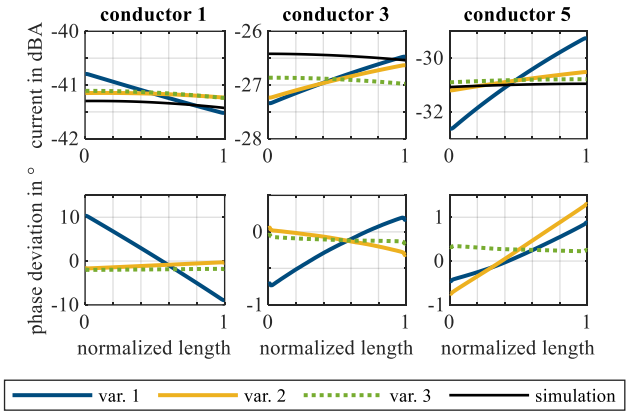

Fig. 5. Given and reconstructed current distribution for 100 MHz using near-field data with phase information.

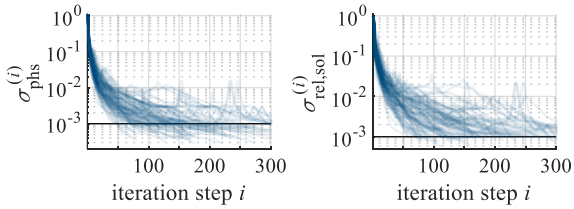

Fig. 6. Development of the criterions defined (16) and (17) of 100 exemplary evaluations of the iterative algorithm for 1 GHz.

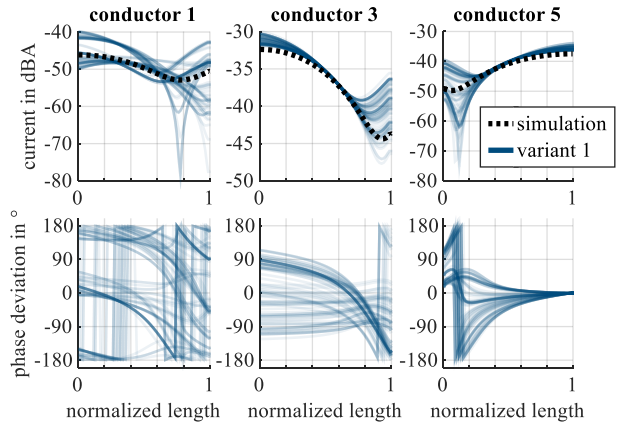

Fig. 7. 100 exemplary results form the iterative algorithm applying variant 1 in constrast to the simulated current distribution for 1 GHz.

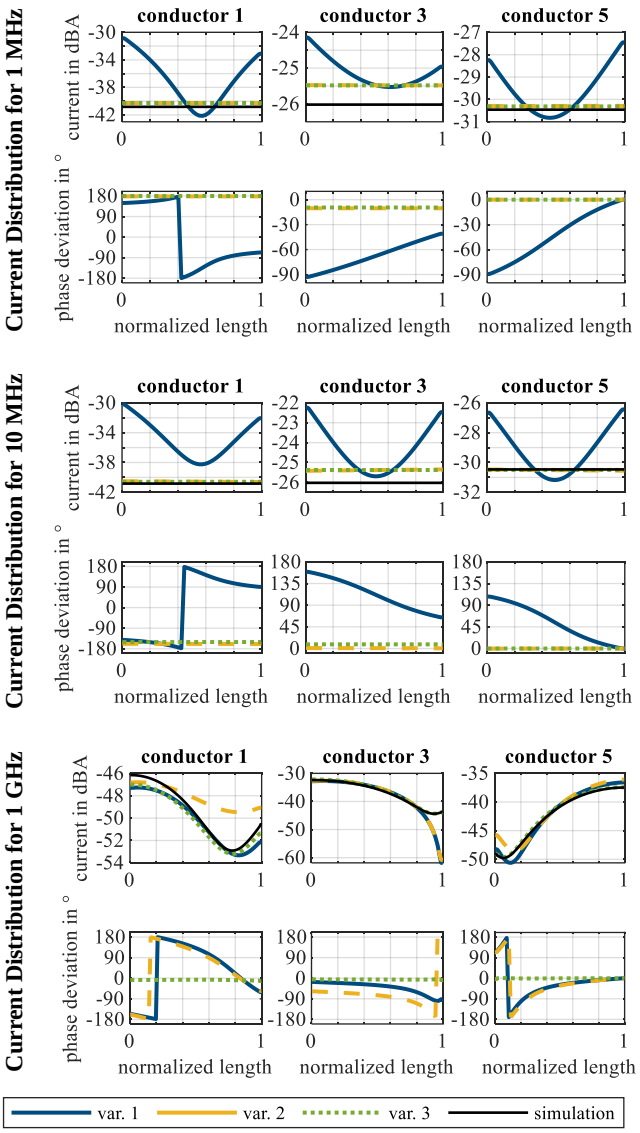

Fig. 8. Reconstructed current distribution for several frequencies using phase-less near-field data

developments of the characteristic criterions defined in (16) and (17) are shown for all 100 evaluations. The found current distribution is presented in comparison to the simulated current distribution in Fig. 7. The superimposed depiction of the results indicates the incidence of several solutions. Almost all evaluations of the iterative algorithm fulfill the stop criterion defined in (26). Especially for conductor 3 and 5, the determined magnitude of the current distributions is close to the reference value. Considering these reconstructed currents, it can be found that the error decreases with increasing magnitudes. So, there is a correlation between the reconstruction quality and the magnitude of the currents. However, there are large deviations of the estimated related phase from the simulation data. Also here, a correlation between magnitude of the currents and quality of the reconstruction can be suggested.

In Fig. 8, one exemplary solution of the iteration algorithm is shown for several frequencies. Initially, the results for 1 MHz and 10 MHz are discussed. For both frequencies, the reconstructed distributions applying variant 2 and 3 fit the expected nearly constant value. In all these presented cases, these reconstructed values are close to the reference value.

However, the phase estimation is not as successful as the magnitude estimation. For conductor 1 the direction of the current flow is completely wrong assumed (phase gap of nearly 180 °). On the other conductors, suitable phase distributions are determined for the investigated frequencies. Nevertheless, the additional conditions of the solution lead to much better results. Here, the usage of termination information (variant 3) is more useful than the limitation of voltages (variant 2). Considering only the network equations (variant 1), the reconstructed distribution tends to form wave phenomena. For much higher frequencies, all variants determine predominantly good results for the magnitude of the current distribution. Using variant 3, the phase information is very close to the reference value. Overall, the comparison of the results for the examined frequencies carves out the usability of the additional conditions in the inverse problem. For lower frequencies, if wave phenomenon cannot be assumed, the consideration of termination information or the limitation of magnitude values leads to much better reconstructions.

D. *Evaluation of the Far-Field*

Knowing the current distribution, the far-field of the investigated conductor system can be estimated. As shown in II, the dipole model can be used to formulate a relation between floating currents and the electric field. Assuming the coordinate $(0.08\,\mathrm{m}, 0.05\,\mathrm{m}, 0\,\mathrm{m})$ as central point of the investigated structure, the electric field is estimated in several distances along the y-axis according to Fig. 4. The observation point is 5 cm above an ideal infinite ground plane. Here, the vertical component of the electric field is dominant. In Fig. 9, the deviation between the estimated and the simulated field from CONCEPT-II is presented. Using current distributions based on additional conditions (variants 2 and 3), the far-field prediction is generally more accurate. Especially for lower frequencies, the usage of additional conditions leads to much better results. Furthermore, using variant 3, the closest estimation is achieved. Knowing the termination impedances, the estimated current distribution seems to be more accurate.

VI. Conclusion and Outlook

In this publication, the current reconstruction method is enhanced using additional conditions. The generally usability is shown. In addition, a simple iterative process based on the reconstruction method is presented that allows the application on phase-less near field data. The wide analysis of the computed results highlights the positive effect on the solution's quality especially for lower frequencies. Finally, the investigation of the estimated far-field represents that the shown approach is potentially useful for EMI-analysis.

Although, the assumption of the termination information is arguable. Often the information about the termination is only approximately and for lower frequencies feasible. However, exactly for this frequency range, the usage of termination information should be possible. In further works, the influence of inaccurate termination information could be evaluated. Also, considering non-linear terminations would be an interesting continuation of this work. Beyond, the current reconstruction should be applied on real phase-less measurement data. Moreover, the prediction of the far-field is just conceptual. The refinement of this model is intended and a comparison to antenna measurement should be done.

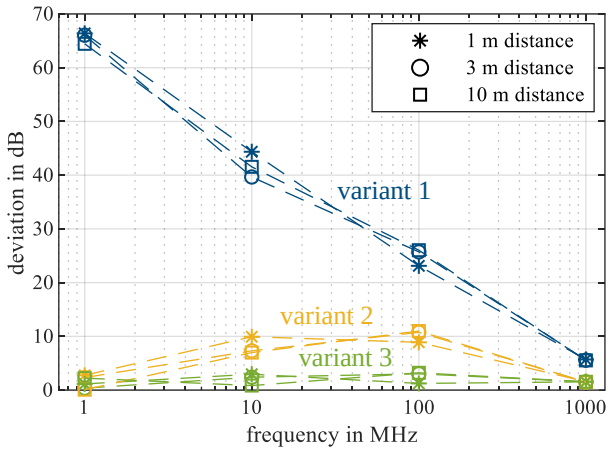

Fig. 9. Deviation of estimated vertical electric field at several distances.

References

[1] J.-R. Regue, M. Ribo, J.-M. Garrell, A. Martin, "A genetic algorithm based method for source identification and far-field radiated emissions prediction from near-field measurements for PCB characterization," *IEEE Trans. Electromagn. Compat.*, vol. 43, no. 4, pp. 520–530, Nov. 2001.

[2] A. Taaghol and T. K. Sarkar, "Near-field to near/far-field transformation for arbitrary near-field geometry utilizing an equivalent magnetic current," *IEEE Trans. Electromagn. Compat.*, vol. 38, no. 3, pp. 536–542, Aug. 1996.

[3] Z. Yu, J.A. Mix, S. Sajuyigbe, K.P. Slattery, J. Fan, "An Improved Dipole-Moment Model Based on Near-Field Scanning for Characterizing Near-Field Coupling and Far-Field Radiation From an IC," *IEEE Trans. Electromagn. Compat.*, vol. 55, no. 1, pp. 97–108, Aug. 2012.

[4] J. Zhang, J. Fan, "Source Reconstruction for IC Radiated Emissions Based on Magnitude-Only Near-Field Scanning," *IEEE Trans. Electromagn. Compat.*, vol. 59, pp. 557–566, April 2017.

[5] Y.-F. Shu, X.-C. Wei, R. Yang, E.-X. Liu, "An Iterative Approach for EMI Source Reconstruction Based on Phaseless and Single-Plane Near-Field Scanning," *IEEE Trans. Electromagn. Compat.*, vol. 60, pp. 937–944, August 2018.

[6] Y. Vives-Gilabert, .C. Arcambal, A. Louis, F.d. Daran, E. Philippe, M. Belahcene, "Modeling Magnetic Radiations of Electronic Circuits Using Near-Field Scanning Method," *IEEE Trans. Electromagn. Compat.*, vol. 49, pp. 391–400, May 2007.

[7] D. Rinas, P. Ahl and S. Frei, "PCB current identification based on near-field meas-urements using preconditioning and regularization," *Adv. Radio Sci.*, vol. 14, pp. 121 – 127, Sept. 2016.

[8] R. Nowak and S. Frei, "Reconstruction of Current Distribution and Termination Impedances of PCB-Traces by Magnetic Near-Field Data and Transmission-Line Theory," in *EMC Europe 2018*, Amsterdamm, 2018, pp. 579 – 584.

[9] Z. Chen, S. Marathe, H. Kajbaf, S. Frei, D. Pommerenke, "Broadband phase resolving spectrum analyzer measurement for EMI scanning applications," in *Proc. IEEE Int. Symp. Electromag. Compat.*, 2015, pp. 1278–1283

[10] H. Zhao, Y. Zhang, J. Hu, E.-P. Li, "Iteration-Free-Phase Retrieval for Directive Radiators Using Field Amplitudes on Two Closely Separated Observation Planes," *IEEE Trans. Electromagn. Compat.*, vol. 58, pp. 607–610, Jan. 2016

[11] C. R. Paul, *Introduction to electromagnetic compatibility*, 2nd ed. Hoboken, NJ, USA: Wiley, 2006.

[12] A. Altman, and J. Gondzio, "Regularized Symmetric Indefinite Systems in Interior Point Methods for Linear and Quadratic Optimization," *Optimization Methods and Software*, vol. 11, pp. 275–302, January 1998.

[13] Institute of Electromagnetic Theory, Hamburg University of Technology (TUHH), Germany. *CONCEPT-II*. (2018) [Online]. Available: http://www.tet.tuhh.de/concept/?lang=en.